Int J Thermophys (2013) 34:1481–1488
DOI 10.1007/s10765-013-1399-x

Ultra-Deep Bone Diagnostics with Fat–Skin Overlayers Using New Pulsed Photothermal Radar

K. Sreekumar · A. Mandelis

Received: 31 January 2012 / Accepted: 15 January 2013 / Published online: 31 January 2013

Abstract The constraints imposed by the laser safety (maximum permissible exposure) ceiling on pump laser energy and the strong attenuation of thermal-wave signals in tissues significantly limit the photothermally active depth in most biological specimens to a level which is normally insufficient for practical applications (a few mm below the skin surface). A theoretical approach for improvement of the signal-to-noise ratio (SNR), minimizing the static (dc) component of the photothermal (PT) signal and making use of the PT radiometric nonlinearity has been introduced. At low frequencies fixed-pulse-width chirps of large peak power were found to be superior to all other equal energy modalities, with an SNR improvement by up to two orders of magnitude. Compared to radar peak delay and amplitude, the long-delayed radar output amplitude is found to be more sensitive to subsurface conditions. Two-dimensional spatial plots of this parameter depicting the back-surface conditions of bones with and without fat tissue overlayers are presented. Pulsed-chirp radar thermography has been demonstrated to monitor the degree of demineralization in goat rib bone with a substantial SNR and spatial resolution that is not practicable with harmonic radars of the same energy density.

Keywords Bone demineralization · Bone diagnostics · Osteoporosis · Photothermal radar · Photothermal radiometry

K. Sreekumar (✉) · A. Mandelis
Centre for Advanced Diffusion-Wave Technologies, Department of Mechanical and Industrial Engineering, University of Toronto, 5 King's College Road, Toronto, ON M5S 3G8, Canada
e-mail: sreekumarkaiplavil@yahoo.co.in

A. Mandelis
e-mail: mandelis@mie.utoronto.ca

1 Introduction

Measurement techniques based on the principles of photo-induced diffusion waves in matter have made remarkable advances in metrology relevant in basic science, engineering, and medical technology [1–3]. Photothermal (PT) techniques, which make use of the principles of diffusion-wave phenomena, basically examine the resulting thermal or acoustic waves, photoexcited charge carriers, phonons, and absorbed or scattered photons in a medium following periodic optical excitation. The successful applications of diffusion-wave science extend over a wide spectrum that covers measurement of thermophysical parameters of solids and fluids [4–7], microscopy and tomography [8–10], wide field imaging and thermography [11,12], non-invasive dental diagnostics [13], microelectronic metrology [14], etc. In medicine and biology, both time- and frequency-domain PT analytical methods have been successful for non-invasive measurements of peripheral and subsurface tissue parameters [15–17]. Imaging of deep lying dental carries has been accomplished with better sensitivity than X-rays (radiographs), with frame synchronized PT wave detection ("dental thermophotonic imaging") [18]. PT imaging of tumors and infections with the aid of nanoparticle contrast agents [19], single bio-molecule identification [20], and nano-cluster assisted cellular imaging [21] are a few among the recent promising applications of PT research in the biomedical field.

The PT radar is a modality that benefits from an improved depth profiling capability compared to conventional PT techniques. This technique is of importance if the specimen of interest contains multiple sources of thermal waves lying at different depths. In contrast to conventional frequency scan techniques that give a depth integrated result, the PT radar yields depth resolved information and thus is ideally suited for probing subsurface interfaces such as bone surfaces with tissue and skin overlayers. Our laboratory [22–24] and other groups [25] have introduced PT cross-correlation (pulse compression) radar techniques, in which the laser modulation is frequency chirped. If $R(\tau)$ and $S(t+\tau)$ are the reference waveform and the responsive signal, respectively, the latter being measured at the delay time t, then the cross-correlation is defined by

$$C_{\mathrm{R}}(t) = \int_{-\infty}^{\infty} R^*(\tau) S(t+\tau) \mathrm{d}\tau. \tag{1}$$

Here $R^*(\tau)$ is the complex conjugate of the reference signal. In the case of multiple sources, at different depths, the conductive component of the PTR signal takes longer than the radiative (emissive) component to reach the surface. When the resulting composite signal is pulse-compressed using correlation with the reference chirp, the output will contain a delayed peak, the delay being a function of the thermophysical properties and the depth of sources below the plane of detection.

While extending the applicability of PT techniques to biological tissues, the major factor of concern is the ability to resolve deep lying absorbers. Reports on using pulsed photothermal radiometry (PPTR) have shown that subsurface absorber detection limits in turbid media and tissue are *ca.* 1 mm [26,27]. However, any successful development of PT diagnostic technologies for bone characterization necessitates capturing

thermal waves generated over a depth of a few millimeter below the skin surface in the soft–hard tissue matrix. Furthermore, laser-induced PT signal quality (SNR) is limited by the ceiling of the safety standard curve for maximum permissible exposure (MPE) with regard to laser power excitation of human tissues [28]. Therefore, any further improvement in PTR depth resolution will have to be associated with substantial SNR enhancement. Relatively low optical absorption in the therapeutic optical window (700 mm to 1300 nm) and strong absorption of infrared (IR) photons by water molecules in tissues make the available depth information carried by the conventional PTR signal at the skin surface too limited for biologically reliable diagnosis. Consequently, development of PT technologies of practical importance for medical applications is very challenging. The recently introduced pulsed-chirp PT radar [24] exhibits much improved SNR and depth profiling capabilities superior to pulsed PTR [26,27] and to the conventional harmonically modulated PTR radar [22,25] for the same optical energy exposure. In this article, we discuss the applications of the pulsed-chirp radar for diagnosing the back-surface defects of bone with tissue overlayers and for imaging the trabecular structure through the cortical layer exploiting its high efficiency and depth profiling capability which is impracticable with conventional PT methods under an equal energy criterion. Also, the technique has been used for monitoring the degree of demineralization in a rib bone through radar thermography seeking the possibility of developing non-ionizing techniques for the early detection of bone osteoporosis.

2 Principle of SNR-Optimized Pulsed Photothermal Radar: Signal and Static Temperature Fields

Both the PT signal (ac) and static temperature rise (dc background) components are examined, the latter being cumulative in nature over several chirp repetition cycles [24]. In agreement with conservation of energy, a method that minimizes the static component would result in a stronger ac component under similar boundary convection and/or radiation heat loss conditions (or if boundary losses are negligible). As long as no phase transitions occur, or radiative energy transfer or photochemical reactions, the energy absorbed by a sample following modulated laser beam excitation will appear both as an ac PT signal and static temperature rise. A fraction of the converted optical-to-thermal energy will also be lost to convection and/or radiation at interfaces. The dc component is found to increase with modulation frequency, the cause of which can be attributed to boundary heat losses for long excitation periods. The characteristic times for building up convective effects for various sample/heating configurations are well documented in the literature [29,30]. The convective loss factor is high if the modulation period is longer than the time for establishing free convection for a sample/experimental configuration which is not perfectly adiabatic. As the frequency increases, the loss factor decreases, leading to a progressive build-up in the static component of the thermal field. Hence, the use of low frequencies would be an effective means to minimize the dc component so that the ac signal will be enhanced. Low frequencies are also consistent with maximizing the thermal-wave depth penetration. A reasonable optical waveform choice to achieve this is a pulse train with a low duty cycle that gives the sample sufficient time to cool down to a temperature as close to

the background as possible between successive pulses. If the pulse repetition period is longer than the boundary surface characteristic loss time, then the dc component or the baseline is greatly reduced, thereby enhancing the modulated signal. Furthermore, since the pulse duration is short, large peak powers can be applied while maintaining low exposure energies within the MPE limits. In PTR, this can be further quantified using Stefan's law, according to which the net energy exchange per unit time of a radiator (sample surface) at temperature T with its surroundings (IR detector) at temperature T_0 (assumed to be the room temperature) is

$$E = \varepsilon\sigma_{\mathrm{SB}}\left(T^4 - T_0^4\right)\ (\mathrm{J}\cdot\mathrm{s}^{-1}). \tag{2}$$

Here ε is the emissivity of the sample surface and σ_{SB} is the Stefan–Boltzmann constant. If the change in temperature of the sample with respect to room temperature is ξ, then

$$E = \varepsilon\sigma_{\mathrm{SB}}\left((T_0+\xi)^4 - T_0^4\right), \tag{3}$$

or, expanding

$$E = 4\varepsilon\sigma_{\mathrm{SB}}T_0^3\xi\left(1 + \frac{3}{2}\left(\frac{\xi}{T_0}\right) + \left(\frac{\xi}{T_0}\right)^2 + \frac{1}{4}\left(\frac{\xi}{T_0}\right)^3\right). \tag{4}$$

It is clear that nonlinearity of Eq. 4 will boost the PTR signal if the temperature rise is not very small compared to the ambient temperature. So, it can be asserted that short-optical pulses of high peak power generate thermal transients of large amplitudes and the resulting PT nonlinearity should improve the SNR. Details of chirp energy calculation and SNR estimation in a comparative manner for various waveforms have been already reported [24]. Under optimum conditions, the SNR of the chirped pulse excitation is higher by two orders of magnitude or more than sine- and square-wave optical excitation.

3 Experimental

The instrumentation details of the multi-waveform PT radar are furnished elsewhere [24]. The pumping source was an 808 nm, 40 W diode laser with fiber delivery. A programmable function generator (Agilent 33200A) coupled with a delay source (Stanford Research DG535) generated the chirp waveforms, which along with the PTR signal from an HgCdTe IR detector was recorded using a high speed data acquisition module (NI 5122). The radar was implemented in a LabView environment with a fast frequency domain algorithm. A pulse duration of 100 μs to 300 μs was found to be ideal in terms of the SNR for bone samples compared to harmonic modulation radars of the same energy. The chirp duration was 5 s and starting and ending frequencies were 0.3 Hz and 1 Hz, respectively. The exposure energy density per chirp for 300 μs pulses is about 25 $\mathrm{mJ}\cdot\mathrm{cm}^{-2}$, which is well within the MPE limit. Compared to conventional

radar parameters (delay time, amplitude, and phase), the output amplitude resulting at long delays (Fig. 1a) is a very responsive marker of subsurface defects. This is in agreement with the fact that immediately after the laser goes off, for an interval which is shorter than the diffusion time, diffusive heat loss is negligible, and the amplitude is controlled by the absorption and forced convection (if any). For a late transient, the curve shape is strongly dependent on the nature thermal diffusion, which is controlled by the boundary conditions. So, the surface/subsurface thermophysical response of the sample is better contained in this region. This long-delay-amplitude (s) has been used to make surface plots of bone with subsurface defects and chemically induced demineralization as well.

A cortical goat bone piece (2 cm × 1.5 cm × 0.3 cm) with a few subsurface holes (0.3 mm radius), drilled across the thickness, was prepared to mimic the mineral-lost condition of the trabecular section (Fig. 2c). The cortical layer thickness above the holes was ∼0.5 mm. It was kept in water for 5 h for better resemblance with a living bone. Both pulsed and sine wave radars (25 mJ · cm^{-2}/chirp) were used to analyze the intact and drilled regions, and the results are shown in Fig. 1. The capacity of long-delay mapping for MPE-optimized bone strength analysis has been further extended to investigate the mineral loss in a goat rib sample. A rib sample (Fig. 3)

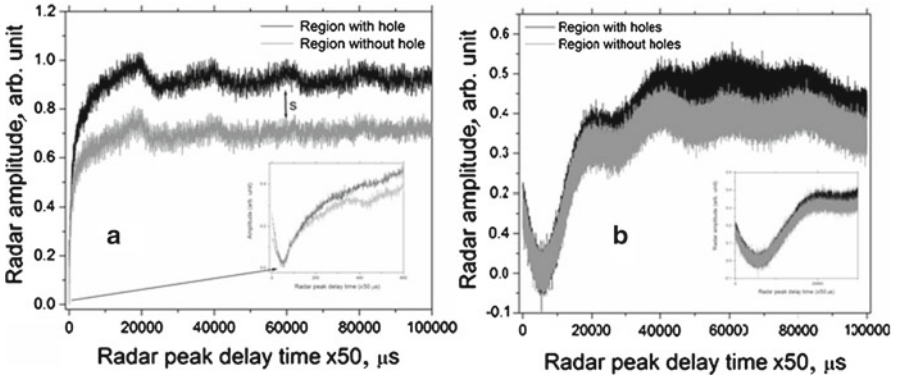

Fig. 1 Radar output with (a) pulsed and (b) sine wave chirps for the regions with and without subsurface holes in a wet bone, at 25 mJ · cm^{-2}/chirp exposure energy. The pulsed radar output is obtained by forcing the valley points (amplitude) to coincide through baseline adjustment. The long-delay-amplitude is designated *s*

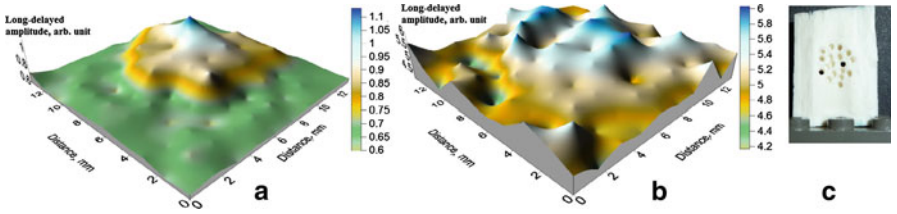

Fig. 2 Long-delay-amplitude (100 ms) images for the wet bone sample with subsurface holes. (a) Without fat-soft tissue and (b) with fat-soft tissue overlayers. Holes are drilled across the thickness from the *bottom*. Scanning step interval is 1 mm along both axes

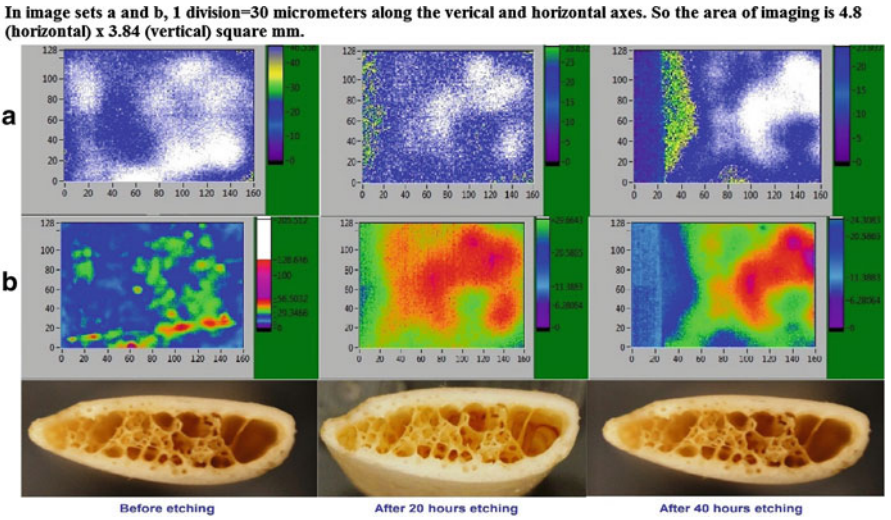

Fig. 3 (a) Harmonic and (b) pulsed radar images of intact and demineralized goat rib for the same energy density. Samples were irradiated on the top surface, which is the plane of imaging

of 3 cm × 1.3 cm × 0.4 cm was subjected to artificial demineralization by dipping in 0.1 N acetic acid solution for 20 h and 40 h. The intact and demineralized samples were imaged using pulsed-chirp radar thermography, in which the single element IR detector was replaced by an IR camera (CEDIP 520M). Image frame dimensions were 160 pixels × 128 pixels, pixel size being 30 μm × 30 μm. Chirp parameters were the same all through the experiments. Images obtained for the correlation amplitude delayed by 100 ms, for harmonic and pulsed radars of chirp energy density 25 mJ · cm^{-2}, are shown in Fig. 3.

4 Results and Discussion

In this study, we have established some key conditions under which PTR measurements of back-surface absorbers/defects in *ex vivo* animal cortical bones simulating the spongy trabecular bone, with overlayers of fat and skin, are possible. In addition, the possibility of monitoring the degree of demineralization using the long-delay radar imaging has been investigated. Maximum signal depth resolution with minimum excitation energy is considered an important optimization factor. The use of chirped pulse optical excitation waveforms of short duration and high peak power has been found to be substantially more advantageous compared to conventional sine- and square-wave excitations. Minimizing the dc baseline and enhancing the radiometric nonlinearity leads to a substantially improved SNR especially at low energies, which facilitate the efficient dissipation of the dc thermal signal baselines. For energies around 10 mJ, the SNR of the chirped pulse excitation is higher by two orders of magnitude or more than sine- and square-wave optical excitation.

Results of the pulsed and sine wave radar amplitude investigation (Fig. 1) on wet bones with subsurface holes clearly indicate the efficiency of the former to discriminate a defective underlayer from healthy portions. We made the valley (minimum in Fig. 1a) points in the radar output for the two regions to coincide, and the resulting difference in amplitude for longer delays (several times the valley/peak delays) was found to be a more responsive parameter compared to conventional indicators such as the peak/valley delay, phase, etc. The pump beam was raster scanned on the front surface of the wet bone, and delayed amplitude maps (Fig. 2) were created. As a simple method to compensate for the influence of the bone surface curvature on the PRT signal, a difference method was considered by recording data before and after drilling holes. The presence of the subsurface damage is detectable with fat ($\sim$0.5 mm thick pig lard) and soft tissue ($\sim$1 mm thick chicken breast) overlayers (Fig. 2b). The delayed amplitude data have been found to be sensitive to bone demineralization as well. As shown in Fig. 3, the pulsed radar images benefit from an improved SNR as well as resolution compared to harmonic excitation of the same energy, which makes clear distinctions for the extent of demineralization.

5 Conclusions

Probing biological structures with the chirped pulse PTR radar was found to be of considerable merit for analyzing *in vitro* multilayer goat bone specimens with deep defects, satisfying major PTR biosensor system criteria such as the MPE laser safety limits and maximum signal quality as measured by an optimal SNR. By virtue of the high pulse compression SNR and suppressed baselines, the chirped pulse PTR radar modality is capable of resolving up to 2.8 mm deep biological structures resembling bone back-surface absorbers, a much higher sensitivity than conventional pulsed-laser PTR which is capable of $<$1 mm depth resolution [24,26]. The long-delay-amplitude which results much later than the peak/valley is more sensitive to subsurface features compared to peak delay or phase, and its significance has been verified on acid-etched and back-surface drilled bones with and without overlayers. Even though distinguishable features due to various layers were observed with the chirped pulse PTR radar, the signal dependence on bone optothermal properties needs further study and exploration.

References

1. A. Rosencwaig, *Photoacoustics and Photoacoustic Spectroscopy* (Wiley, New York, 1980)
2. D.P. Almond, P.M. Patel, *Photothermal Science and Techniques* (Chapman and Hall, London, 1996)
3. A. Mandelis, Phys. Today **53**, 29 (2000)
4. A. Mendioroz, R. Fuente-Dacal, E. Apinaniz, A. Salazar, Rev. Sci. Instrum. **80**, 074904 (2009)
5. J.A. Baldreas-Lopez, A. Mandelis, Rev. Sci. Instrum. **74**, 700 (2003)
6. I.A. Esquef, A. Paula, L. Siqueira, M.G. da Silva, H. Vargas, L.C.M. Miranda, Anal. Chem. **78**, 5218 (2006)
7. M.A. Owens, C.C. Davis, R.R. Dickerson, Anal. Chem. **71**, 1391 (1999)
8. L. Nicolaides, A. Mandelis, Inverse Prob. **13**, 1393 (1997)
9. C. Zhou, T.-H. Tsai, D.C. Adler, H.-C. Lee, D.W. Cohen, A. Mondelblatt, L. Wang, J.L. Connolly, J.G. Fujimoto, Opt. Lett. **35**, 700 (2010)
10. A. Gaiduk, M. Yorulmaz, P.V. Ruijgrok, M. Orrit, Science **330**, 353 (2010)

11. G. Busse, D. Wu, W. Karpen, J. Appl. Phys. **71**, 3962 (1992)
12. G. Busse, J. Phys. Conf. Ser. **214**, 012003 (2010)
13. A. Hellen, A. Matvienko, A. Mandelis, Y. Finer, B.T. Amaechi, Appl. Opt. **49**, 6938 (2010)
14. A. Mandelis, J. Batista, D. Shaughnessy, Phys. Rev. B Condens. Matter **67**, 205208 (2003)
15. T. Wang, S. Mallidi, J. Qiu, L.L. Ma, A.S. Paranjape, J. Sun, R.V. Kuranov, K.P. Johnston, T.E. Milner, J. Biophotonics **4**, 1 (2010)
16. I.A. Vitkin, B.C. Wilson, R.R. Anderson, Appl. Opt. **34**, 2973 (1995)
17. A. Mandelis, C. Feng, Phys. Rev. E Stat. Nonlin. Soft Matter Phys. **65**, 021909 (2002)
18. N. Tabatabaei, A. Mandelis, B.T. Amaechi, J. Biomed. Opt. **16**, 071402 (2011)
19. J.-W. Kim, E.I. Galanzha, E.V. Shashkov, H.-M. Moon, V.P. Zharov, Nat. Nanotechnol. **4**, 668 (2009)
20. D. Lasne, G.A. Blab, S. Berciaud, M. Heine, L. Groc, D. Choquet, L. Cognet, B. Lounis, Biophys. J. **91**, 4598 (2006)
21. V.P. Zharov, V. Galitovsky, P. Chowdhury, J. Biomed. Opt. **10**, 044011 (2005)
22. N. Tabatabaei, A. Mandelis, Rev. Sci. Instrum. **80**, 034902 (2009)
23. A. Mandelis, Rev. Sci. Instrum. **57**, 617 (1986)
24. S. Kaiplavil, A. Mandelis, Rev. Sci. Instrum. **82**, 074906 (2011)
25. R. Mulaveesala, S. Tuli, Appl. Phys. Lett. **89**, 191913 (2006)
26. S.A. Prahl, I.A. Vitkin, U. Bruggemann, B.C. Wilson, R.R. Anderson, Phys. Med. Biol. **37**, 1203 (1992)
27. S. Prahl, in *Life and Earth Sciences, Progress in Photothermal and Photoacoustic Science and Technology*, vol. 3, Chap. 11, ed. by A. Mandelis, P. Hess (SPIE Press, Bellingham, WA, 1997)
28. ANSI Z136.1-2007, American National Standard for Safe Use of Lasers (Laser Institute of America, 2007)
29. H. Straube, O. Breitenstein, J. Appl. Phys. **109**, 064515 (2011)
30. L. Pera, B. Gebhart, Int. J. Heat Mass Transf. **16**, 1131 (1973)